View metadata, citation and similar papers at core.ac.uk

brought to you by CORE

provided by NASA Technical Reports Server

Optical Constants of GaAs-AlGaAs Superlattices and Multiple Quantum Wells

K. B. Kahen and J. P. Leburton

Department of Electrical Engineering and Coordinated Science Laboratory
University of Illinois at Urbana-Champaign
Urbana, Illinois 61801

ABSTRACT

The optical properties of GaAs-$Al_xGa_{1-x}As$ superlattices are calculated as a function of the frequency and superlattice structure. The computations are performed using a partition method which combines the $\vec{k}\cdot\vec{p}$ method with the pseudopotential technique. The influence of the superstructure on the electronic properties of the systems is accounted for by appropriate quantization conditions. We show that the anisotropy and structure dependence of the dielectric constant result mainly from the contribution of the Γ region while the contributions of the other regions of the Brillouin zone are rather insensitive to the superlattice structure. The superlattice index of refraction values are shown to attain maxima at the various quantized transition energies, where for certain structures, the difference between the refractive indices of the superlattice and its corresponding $Al_xGa_{1-x}As$ alloy can be as large as 2%. In general, our results are in good agreement with the experimental data.

PACS Numbers 71.10.+x, 71.25.Tn, 78.20.Bh, and 78.20.Dj

(NASA-CR-176717) OPTICAL CONSTANTS OF GaAs-AlGaAs SUPERLATTICES AND MULTIPLE QUANTUM WELLS (Illinois Univ., Urbana-Champaign.) 24 p HC A02/MF A01 CSCL 20L G3/76

N86-23468

Unclas 09061

I. Introduction

Superlattices and multiple quantum wells have been studied intensively both experimentally and theoretically over the past few years.[1–9] Because of the important optoelectronic applications of these structures,[2,10–11] a large emphasis has been placed on experimentally determining their optical properties.[2,3,9] The majority of the theoretical work has centered on investigating the low energy absorption spectra of these structures;[12–14] while, more general properties, such as the index of refraction, have been practically ignored except for a few recent works.[15–17] However, many applications of superlattices in laser optics are based essentially on the dispersion and optical waveguiding properties of these structures. Since these properties are directly related to the global dependence of the dielectric constant on the electronic structure of these materials, it is the purpose of this paper to provide a general model of the transverse dielectric constant $\epsilon(\omega)$ of superlattices and multiple quantum wells. More specifically, we will investigate the dependence of $\epsilon(\omega)$ on the superstructure parameters.

Sophisticated band structure techniques, such as the pseudopotential[7] and tight binding methods,[4,14] have been used to calculate the dielectric constant of superlattices. The former technique is excellent for short period, ie., a few layers, superlattices; but, has severe computational problems for long period, $\sim$ 100 Å, structures. On the other hand, the tight binding method is valid for long period superlattices; but, is limited to optical phenomena originating around the Γ region. In our method we use our recently developed[18] hybrid band structure technique which combines the $\vec{k}\cdot\vec{p}$ method[19] with a non-local pseudopotential calculation.[20] Energy dependent connection rules at the heterojunctions account for the influence of the superstructure on the electronic properties of the system. In calculating the band structure, we partition the Brillouin zone into the Γ, X, and L regions by expanding the energy bands and matrix elements about these three symmetry points. In order to keep these expressions simple and limited to small basis sets, expansions about the K and W points are also performed and included in the X and L regions. Our technique is computationally fast and can be used to determine the optical properties originating from any

region of the zone. Furthermore, by virtue of treating the symmetry points separately, we are able to obtain a good physical understanding of the parameters which influence the dielectric constant.

Recently,[18] we have shown that about 90-95 % of the low frequency index of refraction of III-V compounds arises from virtual transitions between electronic states at the edges of the Brillouin zone. Given the modifications of the electronic properties caused by the superstructure, it is worthwhile to determine the major influence of the quantization on the contributions of the different regions of the Brillouin zone to the dielectric constant. In this paper we show that the anisotropy and structure dependence of the dielectric constant result mainly from the contribution of the Γ region because of its small conduction band mass; while, the other regions of the zone have a weak structure dependence since the masses are larger and the quantization is nearly randomized. The contributions of these regions to the total dielectric constant are approximately equal to the compositionally averaged alloy values. This result confirms a simplified model developed previously by one of us (JPL).[15]

This paper is organized in the following manner. In Section II we discuss our technique for calculating the superlattice band structure. Included is an account of our partition method and interface connection rules. In Section III we present briefly a formulation of the complex dielectric constant and its extension to incorporate exciton absorption. Since a number of exciton absorption models already exist, our purpose here is only to show that our model can easily incorporate excitons and yield satisfactory results. Finally, in Section IV we briefly examine our results for the absorption coefficient of a GaAs-$Al_xGa_{1-x}As$ superlattice; while, the main emphasis of this section is placed on discussing our results for the index of refraction of various GaAs-AlAs superlattice structures.

II. Superlattice band structure calculation

In long period superlattices, the periodic variation of the band gap causes carrier confinement in the lower energy levels. We account for this carrier confinement by quantizing the z-component of the wavevector $\vec{k}$ which results in a superlattice wavefunction of the form.

$$\Psi_{\vec{k}}=e^{i\vec{k}_{||}\vec{r}_{||}}\Phi^{j}_{K_z}(z)|b> \quad (1)$$

where K_z is the superlattice travelling wavevector in the z-direction, $\vec{r}_{||}$ and $\vec{k}_{||}$ are the position coordinate and wavevector in the plane parallel to the superlattice layers, $|b>$ is the periodic part of the bulk Bloch state, and $\Phi^{j}_{K_z}(z)$ is the envelope wavefunction of the j^{th} quantized state. In this approximation it is assumed that the superlattice periodicity acts only upon the envelope wavefunction in the z-direction. Therefore, the periodic part of the Bloch wavefunction is unchanged from its bulk value and is determined using a $\vec{k}\cdot\vec{p}$ band calculation described in Section IIa. $\Phi^{j}_{K_z}$ is approximated by the wavefunctions sin (k_jz) and cos (k_jz). Consequently, the superlattice band structure differs from the corresponding bulk material band structure only in the quantization direction. In this direction the periodicity of the superlattice produces mini-Brillouin zones which are superimposed upon the larger Brillouin zone of the crystal. We assume the following simplified expression for the energy dispersion relation of the minibands[21]

$$E_j(k_z)=E_j+(-1)^jW_j\cos(k_zd) \quad (2)$$

where E_j and W_j are the midband energy and energy width of the j^{th} miniband, respectively, and d is the period of the superlattice. The superlattice energy dispersion relation is calculated by adding Eq. (2) onto the bulk relations. We obtain the superlattice optical matrix elements between the valence and conduction bands by quantizing the z-component of the $\vec{k}$ vector in the bulk matrix element expressions. Hence,

$$E_B(k_x,k_y,k_z)\rightarrow E_{SL}(k_x,k_y,k_j)+\Delta E_j+(-1)^jW_j\cos(k_zd) \quad (3a)$$

$$M_B(k_x,k_y,k_z)\rightarrow M_{SL}(k_x,k_y,k_j) \quad (3b)$$

where M_B and M_{SL} are the bulk and superlattice matrix elements, respectively, and ΔE_j is the shift in the energy of the j^{th} level resulting from the carrier confinement. The values of k_j, W_j, and ΔE_j are determined using the interface connection rules described below. By applying Eqs. (3) at the three symmetry points, Γ, X, and L, we obtain the quantized electronic band structure presented in Figure 1. Since K and W are low symmetry points, the effects of quantization are negligible for the contributions coming from these regions. Therefore, these contributions are treated in a mean field

approximation where the energy and matrix element dispersion relations are approximately equal to the compositionally averaged bulk alloy values. The alloy values are calculated using the virtual crystal approximation (VCA).[22]

IIa. Bulk band structure calculation

The electronic band structure is obtained by using a hybrid method that we have previously introduced for calculating the optical properties of III-V binary compounds.[18] In this method we partition the Brillouin zone into three regions by expanding the energy bands and matrix elements about the Γ, X, and L symmetry points using the $\vec{k}\cdot\vec{p}$ method. For each symmetry point, a small number of bands are used in each of our $\vec{k}\cdot\vec{p}$ basis sets which results in simple, analytical expressions for the energy bands and matrix elements. Because of the size of the X and L regions, we have supplemented the X and L point expansions by ones about the K and W points. Since K and W are low symmetry points it is difficult to obtain simple $\vec{k}\cdot\vec{p}$ expansions for these points; therefore, their energy and matrix element dispersion relations are obtained directly from a non-local pseudopotential calculation which includes the spin orbit interaction. Using this technique we are able to obtain analytical expressions for the energies and matrix elements at any point in the bulk Brillouin zone which is particularly useful for treating superstructures. The remaining details of the method are given in Ref. 18.

IIb. Interface correction rules

The quantization of the z-component of the $\vec{k}$ vector is obtained by using interface connection rules. Our method for obtaining these rules has the following important features. We assume the continuity of the entire wavefunction and its derivative at the interface, however, since the GaAs-$Al_xGa_{1-x}As$ junction is not abrupt, we average these relations over the length of a unit cell. After carrying out these averages, we recover the usual connection rules[5] of the continuity of F(z) and $\frac{1}{m(E)}\frac{dF(z)}{dz}$ across the interface where F is the envelope wavefunction and m(E) is the energy dependent mass. Here the z-direction is perpendicular to the interface and the mass m(E) is given

by

$$\frac{1}{m(E)}=\frac{1}{m_o}\left[1+\frac{<b_k|\frac{d}{dz}|b_k>}{ik(E)}\right] \tag{4}$$

where m_o is the free electron mass, k(E) is the energy dependent wavevector, and $|b_k>$ is the cell periodic wavefunction obtained using the results of the $\vec{k}\cdot\vec{p}$ expressions discussed previously. Our interface connection rules[23] are, thus, based on the envelope function approximation.[5,8] The advantage of this method is that we incorporate the non-parabolicity of the band structure while the simplicity of the square well potential (Kronig-Penney picture) is preserved. By applying the energy dependent connection rules to a periodic superstructure, we obtain the following relation which is analogous to that of Sai-Halasz et al.,[8] except that now the masses are energy dependent

$$\cos K_z d=\cos k_z^A L_Z \cos k_z^B L_B - Q\sin k_z^A L_Z \sin k_z^B L_B \tag{5a}$$

$$Q=\tfrac{1}{2}\left[\frac{k_z^A m_B(E)}{k_z^B m_A(E)}+\frac{k_z^B m_A(E)}{k_z^A m_B(E)}\right] \tag{5b}$$

where L_Z and L_B are the well and barrier widths of materials A and B, respectively, $d = L_Z + L_B$, and k_z is the wavevector of $\Phi_{K_z}^{j}(z)$ in Eq. (1). In order to evaluate Eqs. (5) it is necessary to determine the energy band offsets at the Γ, X, and L symmetry points. Figure 2 gives these offsets for a GaAs-AlAs interface at 300K assuming a 65:35 Γ point band discontinuity ratio. The values are obtained using experimental data, when available; otherwise, they are estimated from non-local pseudopotential calculations which include spin orbit effects. Eqs. (5) are also valid for $k_{||}\neq 0$ when the quantized energy levels of the different sub-bands are well separated in energy.

III. Dielectric Constant Formulation

The dielectric constant is calculated as the sum of interband optical transitions. Ignoring phonon assisted transitions, the real part of the transverse dielectric constant in the long wavelength limit is given by[24]

$$\epsilon_1(\omega)=1+\frac{8\pi e^2\hbar^2}{m_o^2}\sum_{\vec{k}_i,\vec{k}_f,c,v}\frac{|\hat{e}\cdot P_{cv}(\vec{k})|^2}{(E_{\vec{k}_{f,c}}-E_{\vec{k}_{i,v}})[(E_{\vec{k}_{f,c}}-E_{\vec{k}_{i,v}})^2-\hbar^2\omega^2]} \tag{6}$$

where $P_{cv}(\vec{k}) = <\vec{k}_{f,c}|\vec{p}|\vec{k}_{i,v}>$ is the momentum matrix element between the initial and final states having wavevectors $\vec{k}_i$ and $\vec{k}_f$, respectively, $\hat{e}$ is the unit polarization vector in the direction of the electric field, $E_{\vec{k}_i}$ and $E_{\vec{k}_f}$ are the initial and final states energies, respectively, and ω is the frequency of the electromagnetic field. In Eq. (6) it is assumed that the valence band is filled and the conduction band is empty. The summation over energy bands is restricted to band edge transitions since for optical frequencies, $\hbar\omega < 3eV$, the transition rates between states of higher energy are negligible. As a result of our restriction to band edge transitions, we have to calculate both $\epsilon_1(\omega)$ and $\epsilon_2(\omega)$ because the Kramers-Kronig dispersion relation[24] cannot be used to determine $\epsilon_1(\omega)$ as a function of $\epsilon_2(\omega)$ since $\epsilon_2(\omega)$ is only computed for a limited range of energies. As a consequence of the partition method, the complex dielectric constant is calculated as the sum of the contributions of the Γ, X, and L regions.[18] Once $\epsilon_1(\omega)$ and $\epsilon_2(\omega)$ are known, the absorption coefficient $\alpha(\omega)$ and the index of refraction $n(\omega)$ can be easily determined. Explicit formulas for $\epsilon_2(\omega)$ and $n(\omega)$ are given elsewhere[24] and the remaining details of our dielectric constant formulation are reported in Ref. 18.

IIIa. Exciton Absorption Calculation

The absorption coefficient is related to $\epsilon_2(\omega)$ via the relation[24]

$$\alpha=\frac{\omega\epsilon_2(\omega)}{cn(\omega)} \tag{7}$$

where c is the velocity of light. For absorption due to excitons, there is a bound and a continuum $\epsilon_2(\omega)$ contribution. The bound $\epsilon_2(\omega)$ contribution is given by[14,25]

$$\epsilon_{2\,B}(\omega)=\frac{Cf_o\gamma}{\pi[(E-E_o)^2+\gamma^2]} \tag{8a}$$

$$f_o=|U(\vec{r}=0)|^2|\hat{e}\cdot P_{cv}(0)|^2 \tag{8b}$$

where we have described the b ind exciton peaks by a Lorentzian function with an oscillator

strength f_o and a half width γ, C is a constant factor, and E_o and U(r) are the ground state exciton energy and envelope function, respectively. Since the broadening of the exciton peaks is difficult to model, we have fitted γ so that our theoretical peaks agree with the experimental data. Both E_o and U(r) are calculated using a variational exciton model of Greene et al.[13] We extended this model by making it valid for periodic superstructures and having all of the parameters materially and energy dependent. We calculated the ground state exciton binding energies by subtracting from the variational energies, the energies resulting from Eqs. 5.

For the continuum contribution, we assume a two-dimensional exciton model for which[26]

$$\epsilon_{2,C}(\omega)=\epsilon_{2,F}(\omega)\frac{e^{\pi\alpha}}{\cosh(\pi\alpha)} \tag{9a}$$

$$\alpha=\left|\frac{R}{\hbar\omega-E_o}\right|^{1/2} \tag{9b}$$

where $\epsilon_{2,F}(\omega)$ is the value of $\epsilon_2(\omega)$ without the electron-hole interaction assuming a constant value for $P_{cv}(\bar{k})$ and R is the effective exciton Rydberg.

IV. Results and Discussion:

The absorption coefficient of a GaAs-$Al_{0.5}Ga_{0.5}As$ superlattice with a well and barrier thickness of 85 and 80 Å, respectively, is plotted in Fig. 3. The results are given for light being polarized parallel to the superlattice layers. The solid and dot-dashed lines are the theoretical and experimental[3] values, respectively. Marked on the figure are the quantized Γ point valence band-conduction band transitions which produce the fine structure on the theoretical curve. Since the experimental data have arbitrary units, the data are multiplied by a constant factor such that the two second electron-heavy hole peaks, E_2(e-hh) coincide. The values of γ which are used to fit the five main peaks are ≈ 1,1.3,3, and 9 meV, respectively; while, the calculated binding energies E_o are ≈ 10,10.11.11, and 14 meV, respectively. As can be seen from the figure, our peak positions agree reasonably well with the experimental data, the only discrepancy coming from the E_2(e-lh) peak. The error could result from the use of bulk masses in the plane parallel to the layers. Since

a different mass would change both the binding energy and the continuum position, it is difficult to ascertain qualitatively the overall effect. The sharp rise in the experimental curve for energies greater than $\approx$ 1.75 eV is due to strong indirect transitions in the barrier material induced by alloy scattering. This effect is not included in our present model because the alloy is treated using the VCA. Overall, this figure demonstrates the flexibility of our dielectric constant model and shows the accuracy of our interface connection rule and exciton binding energy models.

Figure 4 gives the contributions of the Γ, X and L regions to the real part of the dielectric constant of a GaAs-AlAs superlattice at $\hbar\omega$ = 1.5 eV for light being polarized parallel and perpendicular to the superlattice layers (solid and dashed lines, respectively). Values are presented as a function of the period $d=L_B+L_Z$ for a mole fraction $x=L_B/(L_Z+L_B)$ of AlAs of 0.3. The superlattice quantization axis is in the [100] direction. Notice the large L contribution with respect to the Γ and X contributions. As already mentioned in a previous paper,[18] this results from the combined effects of large densities of states and momentum matrix elements and small energy gaps present in the L region. The largest contributions come from volumes surrounding the L point and a special $\vec{k}$ point at $\left|\frac{3}{4},\frac{1}{4},\frac{1}{4}\right|$. The X valley also has a high density of states; however, its phase space and marix elements are appreciably smaller than those of the L valley.[18] The L contribution is approximately independent of the period because the superlattice quantization axis is not aligned with any of the principle axes. Hence, in agreement with the experimental findings of Laidig et al.,[27] the effect of the superstructure is only weakly felt at L. The L contribution is isotropic since the x, y, and z directions are all equivalent for the [111] direction. Therefore, for a superlattice grown along the [100] direction, the polarization of the L valleys, as an average over the three orthogonal directions, vanishes in analogy to the bulk case.

The Γ and X contributions both increase as a function of the period. The superlattice structure influences the dielectric constant by determining both the position and miniband width of the lowest quantized energy levels. Each are inverse functions of L_B and L_Z It can be easily determined that the miniband widths have a negligible effect on the dielectric constant. Therefore, the

important factor is the lowering of the quantized levels which results in an increase in ϵ_1 with the period. The peaks on the parallel Γ polarization curve correspond to the first electron-heavy hole and electron-light hole transitions, E_1(e-hh) and E_1(e-lh), respectively. For perpendicular polarization only E_1(e-lh) is present since the symmetry of the heavy hole state precludes momentum matrix elements in the quantization direction. Polarization effects at Γ occur because the heavy hole transitions which are responsible for the strong coupling between the Γ conduction and valence bands are absent for perpendicular polarization.

The X contribution is a weak function of the period because only the conduction band is quantized (we ignore the very small offset between the two valence bands); and, in comparison with the Γ point conduction band mass, both the transverse and longitudinal conduction band masses are large and, thus, rather insensitive to the confinement. Hence, in this case, the dielectric constant assumes approximately its bulk alloy value. For the X region the optical matrix elements are also appreciable only for light polarized along the x and y direction, i.e., similar to the e-hh transition. However, two of the valleys have the superlattice quantization axis parallel to the z-component of the optical matrix elements while the other four valleys have the quantization axis aligned along the y-component of the marix elements. Hence, perpendicular polarization (the quantization axis is perpendicular to the layers) is favored by four of the six X valleys which accounts for the reverse polarization trend for the X valley contribution.

In Figure 5 we compare our results for the normalized index of refraction of a GaAs-AlAs superlattice with the experimental data of Suzuki and Okamoto.[9] Our results are for parallel and perpendicular polarization, solid and dashed line, respectively; while, the experimental data is for parallel polarization, dot-dashed line. The superlattice has a well and barrier thickness of 62 and 27 Å, respectively, and, consequently, $\bar{x} = 0.3$. The experimental data only goes up to $\hbar\omega = 1.8$ eV. Because we have neglected band transitions larger than 6 eV in our model, the results for the bulk GaAs index of refraction are $\approx$ 7% smaller than the experimental values.[28] For most optical transitions, the influence of the higher bands can be described by a constant factor. Therefore, we use a

normalization procedure which enables us to remove this constant contribution and focus only on the band edge transitions. Consequently, in order to compare directly our results with the experimental data, the theoretical and experimental $n(\omega)$ values given in Figs. 5 and 6 are normalized with respect to the theoretical and experimental bulk GaAs index of refraction values at $\hbar\omega = 1.5$ eV, respectively. As in Fig. 3, the theoretical parallel polarization curve is labelled according to the appropriate quantized Γ region transitions. The peaks on the theoretical perpendicular polarization curve are the result of the corresponding light hole and split-off hole transitions indicated on the parallel polarization curve. As discussed previously, there are no heavy hole transitions for perpendicular polarization and the dielectric constant is larger for parallel polarization. However, notice that the anisotropy vanishes around 2.3 eV due to the falling off of the Γ contribution and the isotropy of the L contribution.

As can be seen from the figure, our results compare favorably with the experimental data, there being less than a 2 % discrepancy between the two parallel polarization curves. Our E_1(e-hh) peak is shifted to higher enegies by $\approx$ 8 meV and is slightly larger. The slight shift could result from the uncertainties in the AlAs band structure parameters and in the Γ point band discontinuity ratio,[29] both of which affect the position of the transition. Both the E_1(e-lh) and E_2(e-hh) peaks are absent from the experimental data. The light hole transitions are barely noticeable on our parallel polarization curve, being weak and overshadowed by the neighboring e-hh transitions; consequently, they might be difficult to observe experimentally. We do not know why the E_2(e-hh) peak is absent from the experimental data. However, in general the data verify the validity of our superlattice model.

In Figure 6 we give the normalized index of refraction at 1.5 eV for a range of GaAs-AlAs superlattices. Again, the solid and dashed lines are for light being polarized parallel and perpendicular to the superlattice layers, respectively. Also shown in the figure are the normalized experimental alloy values[28] corresponding to four of the five superlattice compositions (there is no data for $x = 0.6$). As in Figure 4, the main peaks on the curves correspond to the quantized Γ region

transitions. All of the parallel polarization curves exhibit the E_1(e-hh) peak while the x = 0.1 and 0.2 curves also show the E_2(e-hh) peak. Again for perpendicular polarization, the peaks are due to the E_1(e-lh) transition. The E_1(e-lh) transition also contributes to the parallel curves; however, it is barely noticeable, being overshadowed by the neighboring E_1(e-hh) peak as in the previous figure. For both polarizations the peaks become larger and narrower up to x = 0.3, after which they become smaller. These effects can be explained by the following mechanisms. For small x values the peaks are broad because a large change in the period is required to modify the superlattice characteristics which resemble those of bulk GaAs. Additionally, the effects of quantization are weakly felt for these structures which results in shallower peaks. For larger x values, the superlattice properties are a stronger function of the period which produces sharper peaks; however, with increasing AlAs content, the peaks become shallower because the AlAs Γ region contribution is approximately a factor of seven times smaller than that of GaAs.[18]

A characteristic feature of all of the curves is the shift in the peak positions for increasing AlAs content. For any mole fraction x, the energy of an optical transition increases as a function of the barrier width, but, decreases more rapidly with the well width; consequently, the transition energies are the largest for small period superlattices because of the strong confinement. Therefore, as the period d increases for constant x, the transition energy decreases (weakening confinement since L_Z increases) and a peak occurs when the energy crosses the 1.5 eV level. Also, as x increases for a constant value of the period, the transition energy increases since L_B is increasing while L_Z is decreasing (AlAs has a larger band gap than GaAs). Therefore, larger L_Z values, i.e., the shift in the peaks for increasing x, are required to reduce the transition energy to the value of 1.5 eV. This explains why the curves with the smallest barrier values, x = 0.1 and 0.2, also contain the E_2(e-hh) transition and why the x = 0.6 curve for perpendicular polarizaion does not exhibit the E_1(e-lh) transition.

Another feature of the curves is the strong polarization effect which weakens with increasing AlAs content. Parallel polarization is favored since the superlattice Γ contribution is more aniso-

tropic than the X contribution. The reduction in anisotropy occurs because of the smaller AlAs Γ region contribution, as explained previously.

The most important point to notice in Figure 6 is the positions of the alloy index of refraction values relative to those of the superlattices. For parallel polarization it can be seen that the difference between the alloy and superlattice index of refractions increases with x and with L_B, i.e., with the period. The later trend is in agreement with the experimental findings of Suzuki and Okamoto[9] and confirms the conjecture of Holonyak et al.[10] about the difference in the index of refractions of a superlattice and its corresponding alloy. Figure 6 also shows that this difference is largest at the quantized transition energies and can be as high as $\approx$ 3.5% for specific superlattice structures. In our calculations, an optimal value is achieved for a structure characterized by $L_Z \approx$ 79 Å and $L_B \approx$ 40 Å. However, because our model overestimates $n(\omega)$ by $\approx$ 1.5% with respect to the experimental superlattice values, a more accurate estimate of the difference between the index of refractions of the two structures is $\approx$ 2%. Optical waveguiding can already occur using an index step of $\approx$ 0.00628 (assuming a symmetric AlGaAs planar waveguide with a thickness of 2 μm and $\hbar\omega$ = 1.5 eV);[30] whereas, here we show that with certain structures a step of $\approx$ 0.07, i.e., a factor of 10 larger, can be obtained. Consequently, the waveguiding and reflectance properties of optoelectronic devices which incorporate superlattices can be drastically improved by tailoring the structure to the chosen optical frequency.

V. Conclusion

The band structure partition method that we have previously developed for studying the optical properties of III-V binary compounds has been shown to be successful also for superlattices. The quantization of the electronic states caused by the superstructures has been incorporated into our model within the envelope-function approximation and derived using energy dependent connection rules at the layer interfaces.

The results of our model for the index of refraction and absorption coefficient of GaAs-AlGaAs superlattices are in good agreement with the experimental data. We have shown that the anisotropy and structure dependence of the dielectric constant result mainly from the Γ region because of the small conduction band mass; while, the outer regions (X and L) of the Brillouin zone provide contributions which are similar to the corresponding alloy values. These results confirm the validity of our earliest model and verify its simplifying assumptions.[15] In comparison with the index of refraction of the corresponding $Al_xGa_{1-x}As$ alloy, characterized by the same average mole fraction x of AlAs, our results indicate that the superlattice index of refraction values attain maxima at the various quantized transition energies, where for certain structures the difference can be as large as 2%.

Acknowledgements:

The authors are indebted to K. Hess and N. Holonyak, Jr., for encouragement and helpful discussions. The support of the National Aeronautics and Space Administration is gratefully appreciated.

References

1. L. Esaki and R. Tsu, IBM J. Res. Dev. *14*, 61 (1970).

2. N. Holonyak, Jr., R. M. Kolbas, R. D. Dupuis, and P. D. Dapkus, IEEE J. Quant. Elect. *QE-16*, 170 (1980).

3. S. W. Kirchoefer, N. Holonyak, Jr., K. Hess, D. A. Gulino, H. G. Drickamer, J. J. Coleman, and P. D. Dapkus, Appl. Phys. Lett. *40*, 821 (1982).

4. J. N. Schulman and T. C. McGill, Phys. Rev. Lett. *39*, 1680 (1977).

5. D. J. Ben Daniel and C. B. Duke, Phys. Rev. *152*, 683 (1966).

6. E. Caruthers and P. J. Lin-Chung, Phys. Rev. Lett. *38*, 1543 (1977).

7. J. Ihm, P. K. Lam, and M. L. Cohen, Phys. Rev. B *20*, 4120 (1979).

8. G. A. Sai-Halasz, R. Tsu, and L. Esaki, Appl. Phys. Lett. *30*, 651 (1977).

9. Y. Suzuki and H. Okamoto, J. Elect. Mater. *12*, 397 (1983).

10. N. Holonyak, Jr., W. D. Laidig, M. D. Camras, J. J. Coleman, and P. D. Dapkus, Appl. Phys. Lett. *39*, 102 (1981).

11. W. D. Laidig, N. Holonyak, Jr., M. D. Camras, K. Hess, J. J. Coleman, P. D. Dapkus, and J. Bardeen, Appl. Phys. Lett. *38*, 776 (1981).

12. R. C. Miller, D. A. Kleinman, W. T. Tsang, and A. C. Gossard, Phys. Rev. B *24*, *1134 (1981)*.

13. R. L. Greene, K. K. Bajaj, and D. E. Phelps, Phys. Rev. B *29*, 1807 (1984).

14. Y. C. Chang and J. N. Shulman, Phys. Rev. B *31*, 2069 (1985).

15. J. P. Leburton and K. Hess, J. Vac. Sci. Tech. B *1*, 415 (1983).

16. K. B. Kahen, J P. Leburton, and K. Hess, Superl. Microst. *1*, 289 (1985). In this earlier version of our superlattice dielectric constant model, we used a simpler model for the X and L region contributions and assumed an 85:15 Γ point band discontinuity ratio.

17. K. B. Kahen and J. P. Leburton, Appl. Phys. Lett. *47*, 508 (1985).

18. K. B. Kahen and J. P. Leburton, Phys. Rev. (in press).

19. E. O. Kane, J. Phys. Chem. Solids *1*, 82 (1956).

20. J. R. Chelikowsky and M. L. Cohen, Phys. Rev. B *14*, 556 (1976).

21. B. R. Nag, in *Electron Transport in Compound Semiconductors*, ed. by H. J. Queisser (Springer-Verlag, New York, 1980),Vol. 11, p. 52.

22. J. M. Ziman, *Models of Disorder* (Cambridge University Press, Cambridge, 1977).

23. J. P. Leburton and K. Kahen, Superl. Microst. *1*, 49 (1985).

24. R. Bassani and G. P. Parravicini, *Electronic States and Optical Transitions in Solids*, (Pergamon Press, Oxford, 1975), Chapt. 5.

25. D. F. Blossey, Phys. Rev. B *10*, 3976 (1970).

26. M. Shinada and S. Sugano, J. Phys. Soc. Japan *21*, 1936 (1966).

27. W. D. Laidig, D. K. Blanks, and J. F. Schetzina, J. Appl. Phys. *56*, 1791 (1984).

28. H. C. Casey, Jr., D. D. Sell, and M. B. Panish, Appl. Phys. Lett. *24*, 63 (1974).

29. H. Okumura, S. Misawa, S. Yoshida, and S. Gonda, Appl. Phys. Lett. *46*, 377 (1985).

30. R. G. Hunsperger, *Integrated Optics: Theory and Technology* (Springer-Verlag, New York, 1982), p. 35.

Figure Captions

Fig. 1. Band structure of GaAs and the effect of quantization on each of the symmetry points.

Fig. 2. Energy band offsets at 300 K at each of the symmery points for a GaAs-AlAs superlattice. The energy levels are calculated assuming a 65:35 Γ point band discontinuity ratio. Each level is marked with the appropriate double group symmetry notation.

Fig. 3. Relative absorption of a GaAs-$Al_{0.5}Ga_{0.5}As$ superlattice for parallel polarization at 300 K. The solid and dot-dashed lines are the theoretical and experimental values, respectively. The arrows mark the positions, relative to the theoretical curve, of the Γ valley transitions. e-hh(j) corresponds to a transition between the j^{th} level of the heavy hole band and the j^{th} level of the lowest conduction band.

Fig. 4. Structure dependence of the Γ, X, and L region contributions to the real part of the dielectric constant of a GaAs-AlAs superlatice at $\hbar\omega$ = 1.5 eV. The mole fraction of AlAs in the structure is x = 0.3 and a_o is the lattice constant. Solid line: electric field polarization vector parallel to the superlattice layers. Dashed line: electric field polarization vector perpendicular to the superlattice layers. Note that the L region contribution is isotropic.

Fig. 5. Normalized index of refraction of a GaAs-AlAs superlattice as a function of frequency. The solid and dot-dashed lines are the theoretical and experimental parallel polarization values, respectively, and the dashed curve gives the theoretical perpendicular polarization values. The arrows mark the positions of the quantized Γ valley transitions. e-hh(j) corresponds to a transition between the j^{th} level of the heavy hole band and the j^{th} level of the lowest conduction band.

Fig. 6. Structure dependence of the normalized index of refraction at 1.5 eV for a number of GaAs-AlAs superlattice structures. The solid and dashed lines are for light being polarized parallel and perpendicular to the layers, respectively, and a_o is the lattice constant. The arrows on the left side of the figure mark the positions of the normalized

experimental alloy values for the indicated mole fractions x of Al. The mole fractions given on the right side of the figure belong to the adjacent parallel polarization curve; whereas, for perpendicular polarization, the indicated mole fractions correspond to the curves in descending order.

Fig. 1

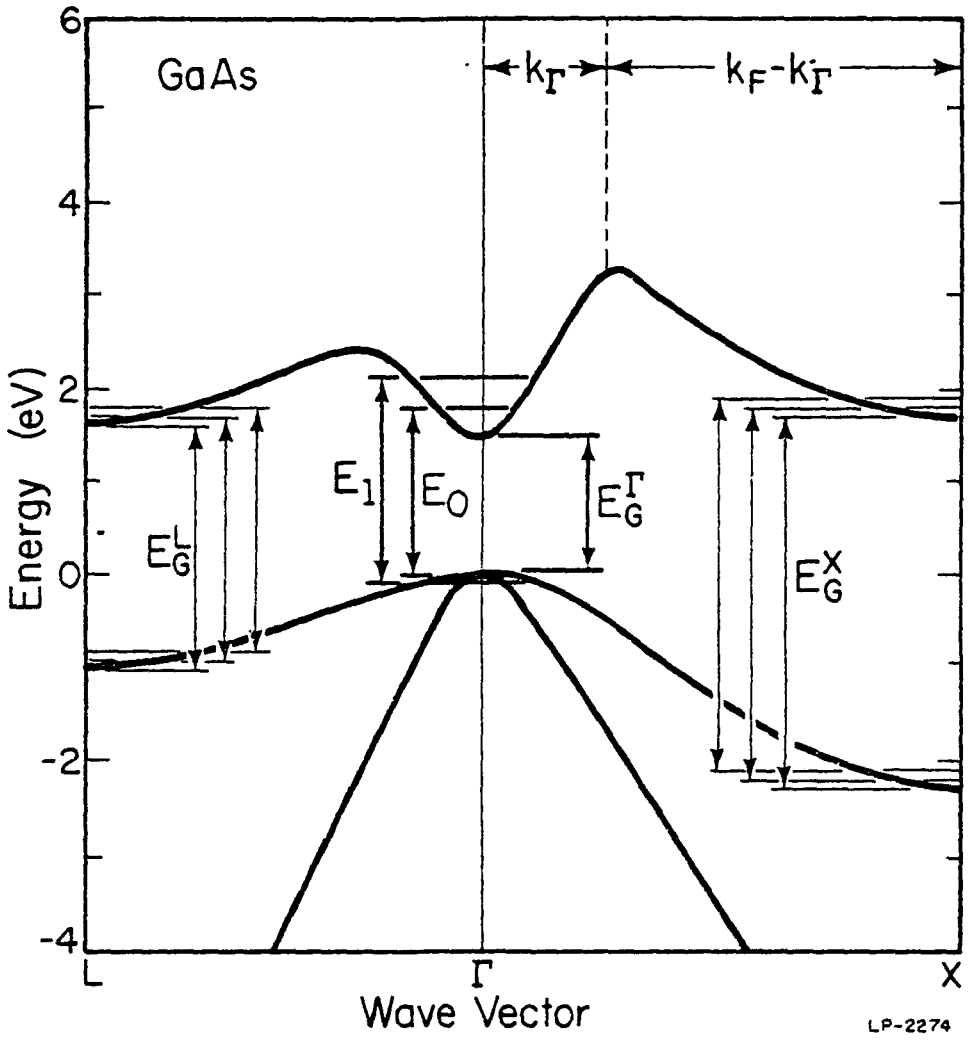
GaAs
k_Γ
$k_F - k_\Gamma$
6
4
2
0
-2
-4
Energy (eV)
E_1
E_0
E_G^Γ
E_G^L
E_G^X
L
Γ
X
Wave Vector
LP-2274

Fig 2

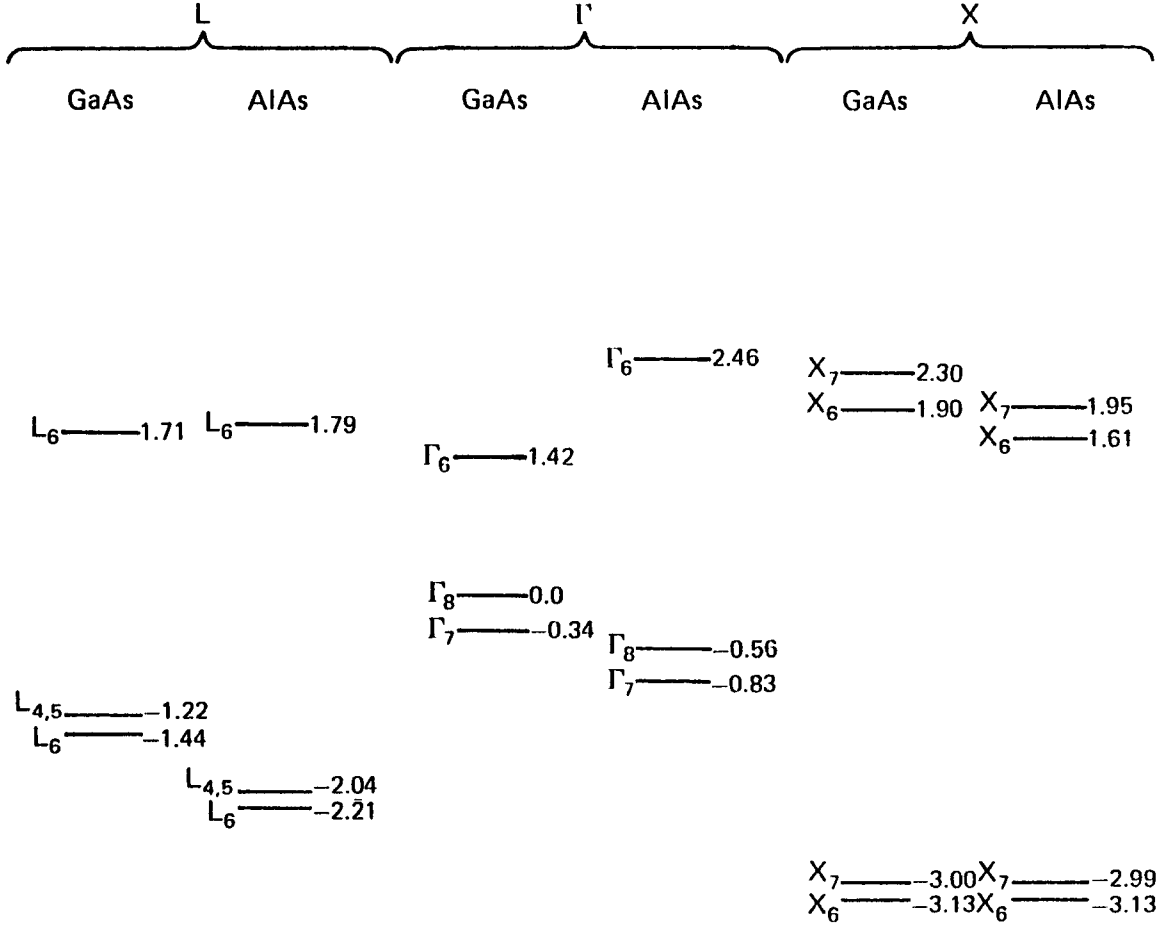
L
Γ
X
GaAs
AlAs
GaAs
AlAs
GaAs
AlAs
Γ6 2.46
X7 2.30
X6 1.90
X7 1.95
X6 1.61
L6 1.71
L6 1.79
Γ6 1.42
Γ8 0.0
Γ7 −0.34
Γ8 −0.56
Γ7 −0.83
L4,5 −1.22
L6 −1.44
L4,5 −2.04
L6 −2.21
X7 −3.00
X6 −3.13
X7 −2.99
X6 −3.13
LP−2542

Fig. 3

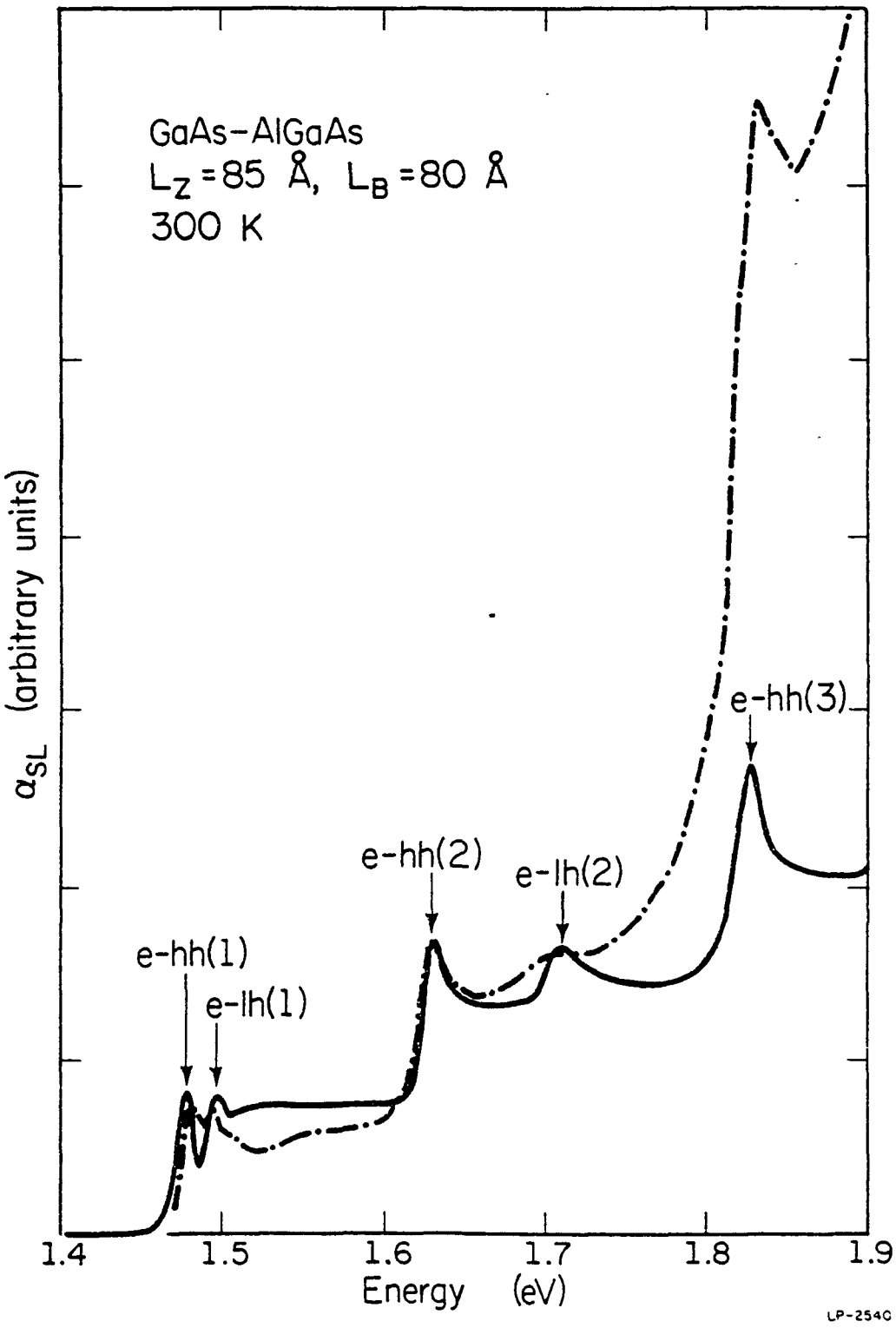
GaAs–AlGaAs
L_Z = 85 Å, L_B = 80 Å
300 K
α_{SL} (arbitrary units)
e-hh(1)
e-lh(1)
e-hh(2)
e-lh(2)
e-hh(3)
1.4
1.5
1.6
1.7
1.8
1.9
Energy (eV)
LP-2540

Fig 4

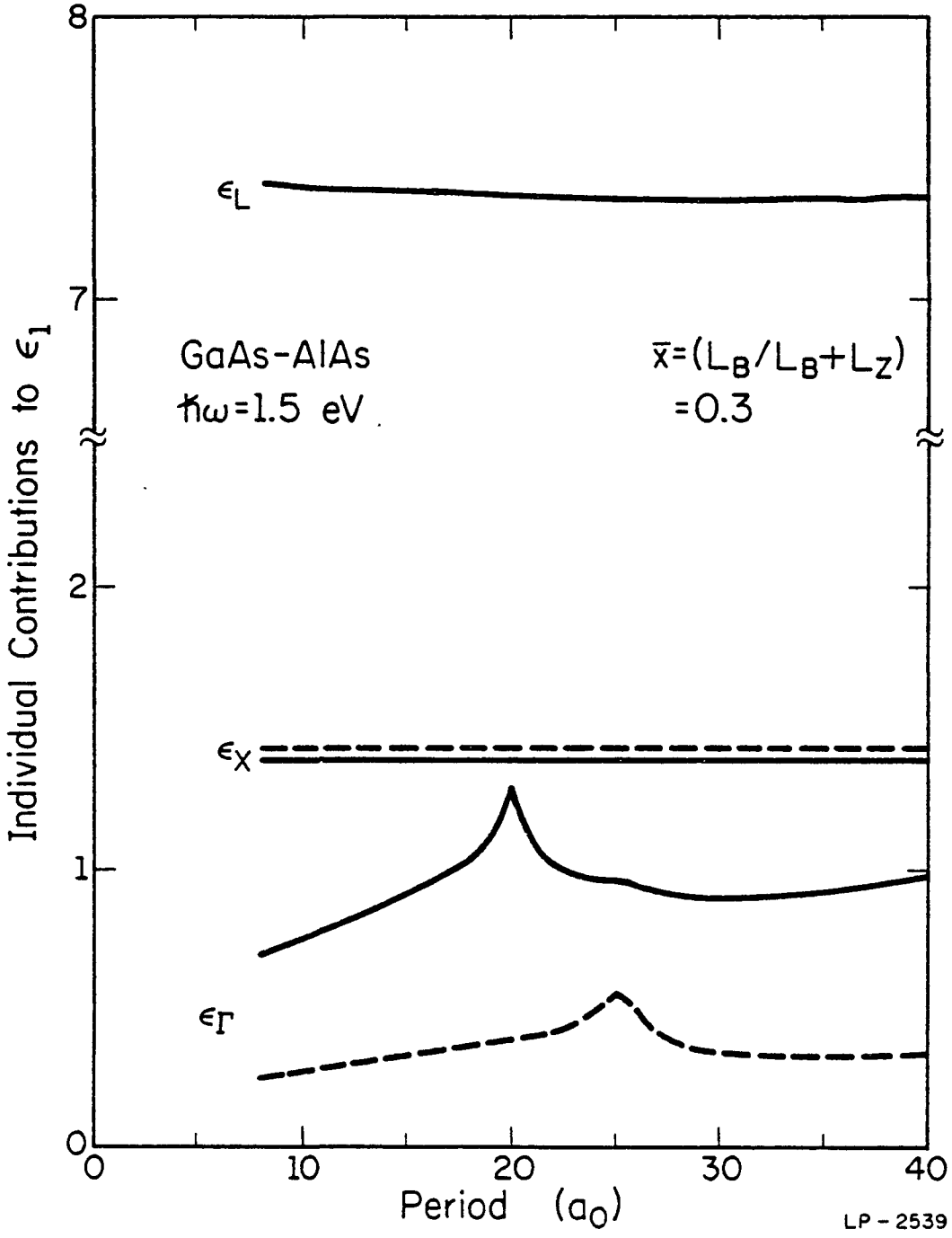
8
7
2
1
0
0
10
20
30
40
Period (a0)
Individual Contributions to ε1
εL
εX
εΓ
GaAs-AlAs
ħω=1.5 eV
x̄=(LB/LB+LZ)
=0.3
LP - 2539

Fig. 5

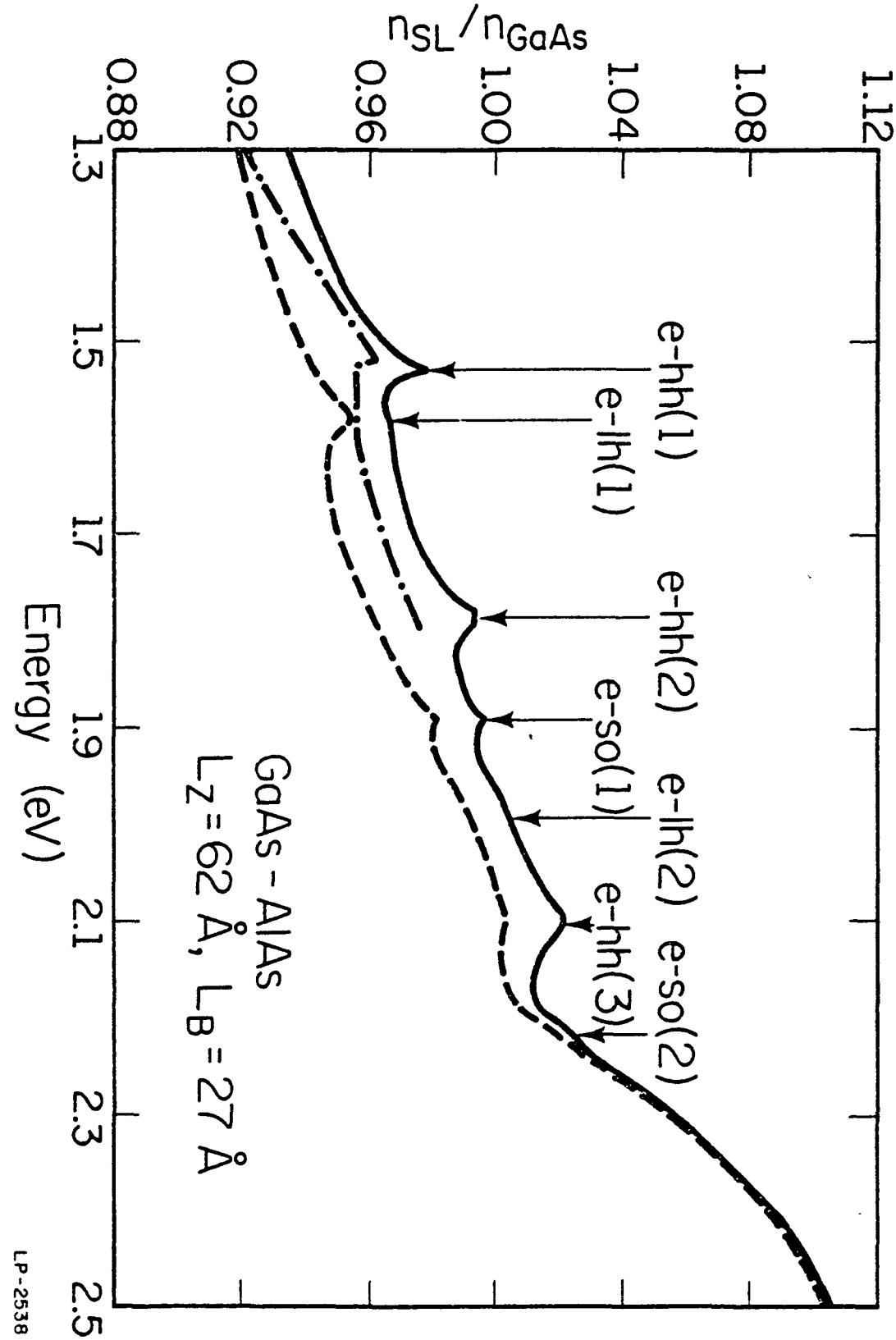
n_{SL}/n_{GaAs}
0.88
0.92
0.96
1.00
1.04
1.08
1.12
1.3
1.5
1.7
1.9
2.1
2.3
2.5
Energy (eV)
e-hh(1)
e-lh(1)
e-hh(2)
e-so(1)
e-lh(2)
e-hh(3)
e-so(2)
GaAs - AlAs
L_z = 62 Å, L_B = 27 Å
LP-2538

Fig. 6

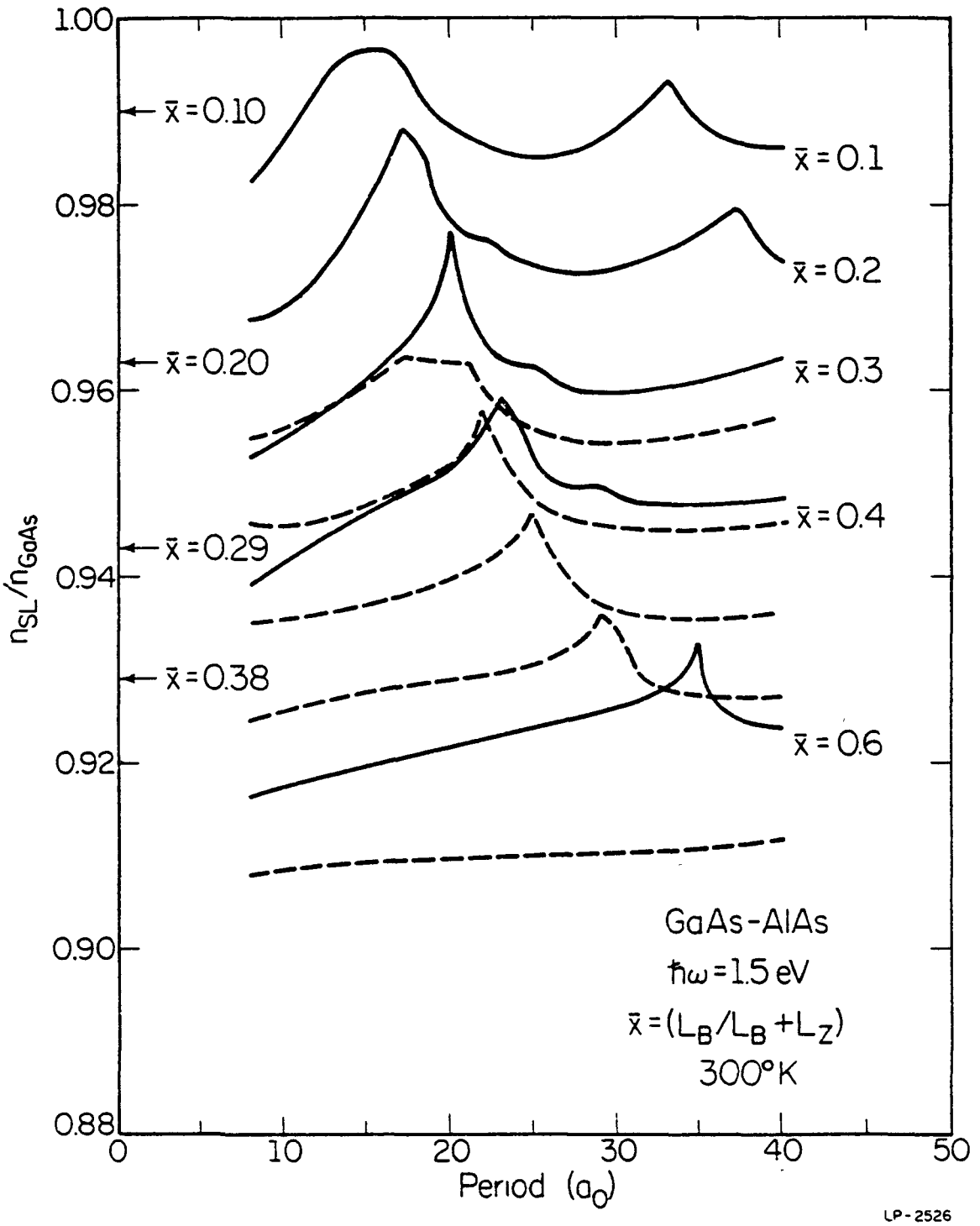
1.00
0.98
0.96
0.94
0.92
0.90
0.88
n_{SL}/n_{GaAs}
$\bar{x}=0.10$
$\bar{x}=0.20$
$\bar{x}=0.29$
$\bar{x}=0.38$
$\bar{x}=0.1$
$\bar{x}=0.2$
$\bar{x}=0.3$
$\bar{x}=0.4$
$\bar{x}=0.6$
GaAs-AlAs
$\hbar\omega=1.5$ eV
$\bar{x}=(L_B/L_B+L_Z)$
300°K
0
10
20
30
40
50
Period (a_0)
LP-2526